A Measurement of Beauty Photoproduction Through Decays to Muons and Jets at HERA-II

H1 Collaboration

Abstract

The photoproduction of beauty quarks in ep collisions has been measured using a data sample of $170\,\mathrm{pb}^{-1}$ collected with the H1 detector at HERA-II in the years 2006 and 2007. This measurement follows closely a measurement performed at HERA-I, where beauty photoproduction events were investigated with two jets and a muon in the final state, and beauty events were identified using the muons relative transverse momentum to a jet and its impact parameter. Visible cross sections were measured differentially in the transverse momenta of the highest energy jet ($p_{\mathrm{T}}^{\mathrm{jet1}}$) and the muon ($p_{\mathrm{T}}^{\mu}$), the pseudorapidity of the muon (η^{μ}) and of the photon's momentum fraction $x_{\gamma}^{\mathrm{obs}}$ entering the hard interaction. The measurements are found to be well described by QCD calculations at NLO.

1 Introduction

The production of beauty quarks in ep collisions has been investigated in considerable detail at HERA-I. In several analyses it was observed that measured cross sections where significantly above the predictions from perturbative QCD calculations in next-to-leading order (NLO). The data from HERA-II with its larger statistics makes it possible to repeat these measurements with increased accuracy.

This measurement follows closely a measurement performed with data from HERA-I [1], where beauty photoproduction events were investigated with two jets and a muon in the final state. Visible cross sections were measured differentially in the transverse momenta of the highest energy jet ($p_{\rm T}^{\rm jet1}$) and the muon ($p_{\rm T}^{\mu}$), the pseudorapidity of the muon (η^{μ}) and of the photon's momentum fraction $x_{\gamma}^{\rm obs}$ entering the hard interaction.

The result of the HERA-I measurement was that NLO calculations describe the data reasonably well, except for the lowest bin of the muon and jet transverse momentum, $p_{\rm T}^{\mu}$ and $p_{\rm T}^{\rm jet1}$, where the data were significantly above the predictions. A similar measurement has also been made by the ZEUS collaboration [2], in a similar but not identical phase space. Here, good agreement was found with QCD predictions, also at low jet and muon $p_{\rm T}$.

The measurement presented here uses the HERA-II data set to measure the same cross sections as in the previous H1 publication with increased statistics and correspondingly smaller errors. In addition, the differential cross section as a function of the azimuthal angle difference $\delta\phi_{\rm jets}$ between the two leading jets has also been measured.

2 Data Sample

The data was collected with the H1 detector in the years 2006 and 2007, when HERA collided electron and positron beams of an energy of $E_{\rm e} = 27.55\,{\rm GeV}$ with protons of $E_{\rm p} = 920\,{\rm GeV}$.

A detailed description of the H1 detector can be found elsewhere [3]. The main components utilized in this analysis were the Central Jet Chamber (CJC), the Liquid Argon Calorimter (LAr), the rear Spaghetti Calorimeter (SpaCal) [4], the Central Muon Detector (CMD), the Central Silicon Tracker (CST) [5] and the Fast Track Trigger (FTT) [6].

The total integrated luminosity corresponds to $170\,{\rm pb}^{-1}$, of which $49\,{\rm pb}^{-1}$ were collected in the year 2006 running with electrons, and $121\,{\rm pb}^{-1}$ were collected in the years 2006/07 running with positrons.

The events were triggered on the first trigger Level by demanding a track segment in the muon system and track activity in the central jet chamber.

3 QCD Models

The Monte Carlo generators PYTHIA 6.2 [7] and Cascade 2.0 [7] were used for the simulation of signal and background distributions. Event samples from both generators were simulated with a detailed detector simulation based on GEANT [8] and subjected to the same reconstruction program as real data.

The PYTHIA event samples were generated in an inclusive production mode (`MSTP(14)=30`), where direct and resolved processes are calculated using massless matrix elements. The CTEQ6L [9] and SAS-1D [10] parton density sets were used for the proton and the photon, respectively. The fragmentation of heavy quarks to hadrons was simulated using the fragmentation function by Peterson *et al.* [12] with a parameter $\epsilon_{\mathrm{b(c)}} = 0.0069(0.058)$ for beauty (charm) quarks. More details on the parameter settings can be found in our previous publication [1].

For cross checks, additional Monte Carlo samples were generated using the Cascade program, which in contrast to PYTHIA is based on k_{T} factorization and the CCFM evolution rather than collinear factorization and DGLAP evolution. The proton parton density set A0 [11] is used for the unintegrated gluon density in the proton.

Both programs, PYTHIA and Cascade, use Leading Order (LO), i.e. $O(\alpha_{\mathrm{s}})$, QCD matrix elements for the hard scattering, augmented by parton showers that approximate the effect of additional multiple gluon emission.

To compare the data to Next-to-Leading Order (NLO) QCD, i.e. $O(\alpha_{\mathrm{s}}^2)$, the FMNR program [13] has been used, which is based on the NLO calculation by Nason, Dawson, and Ellis [14]. This program provides weighted events with two or three partons that result from the hard interaction, but no parton showers. The implementation of beauty hadron formation and decay to leptons is described in our earlier publication [1]. The parton states were subjected to the same jet algorithm as the hadrons in the PYTHIA and Cascade event samples, to form observables (in particular, the p_{T} of the most energetic jet $p_{\mathrm{T}}^{\mathrm{jet1}}$, $x_{\gamma}^{\mathrm{obs}}$, and $\delta\phi_{\mathrm{jets}}$) on parton level. We have used the CTEQ5F4 [16] (GRV-G HO [17]) parton density set for the proton (photon).

Hadronisation corrections were calculated using the PYTHIA program; for events generated with PYTHIA, the jet related observables were calculated once using the final state partons, and a second time from the resulting hadrons. From this, for each observable a migration matrix was determined that describes how the events in bins of the parton level observables migrate to the hadron level bins. This is a refinement of the procedure used in our previous publication [1], where only the bin-by-bin ratio of events on parton and hadron level was determined and applied to the parton level distributions. The resulting differences in the predicted hadron level cross sections are, however, minor compared to the theoretical uncertainties.

The theory uncertainties were determined by varying the input beauty mass[1] m_{b} from the nominal value $m_{\mathrm{b}} = 4.75\,\mathrm{GeV}$ up and down by $0.25\,\mathrm{GeV}$. In addition, the renormalization and factorization scales μ_{r} and μ_{f} were varied independently in the range $\mu_0/2 \leq \mu_{\mathrm{r}}, \mu_{\mathrm{f}} \leq 2\,\mu_0$, with the constraint $1/2 \leq \mu_{\mathrm{r}}/\mu_{\mathrm{f}} \leq 2$. This is the procedure adopted by the HERA-LHC

---

[1]The QCD calculation uses the pole mass. The most recent evaluation by the Particle Data Group [15] yields $\overline{m}_{\mathrm{b}} = 4.20 \pm 0.07\,\mathrm{GeV}$ for the $\overline{\mathrm{MS}}$ running mass, corresponding to $m_{\mathrm{b}} = 4.80 \pm 0.07\,\mathrm{GeV}$ for the pole mass. Here, we continue to use the mass range $m_{\mathrm{b}} = 4.75 \pm 0.25\,\mathrm{GeV}$ for better comparison with other publications.

workshop [18, p. 406]. This is again a refinement compared to our previous publication, where μ_r and μ_f were kept equal and were varied at the same time as the beauty mass. For each bin on hadron level, the deviations due to the beauty mass variation and the largest deviation due to the scale variation in the upward and downward direction were determined and added in quadrature for the total model uncertainty, following the prescription in [18].

4 Analysis Method

Events were selected with the following experimental cuts:

- No electron candidate with an energy above $E > 6\,\mathrm{GeV}$ is allowed to be found in the detector. This removes most deep inelastic scattering (DIS) events with a momentum transfer Q^2 of $Q^2 \gtrsim 2.5\,\mathrm{GeV}^2$. Monte Carlo simulations were used to correct for the remaining DIS background with $Q^2 > 1\,\mathrm{GeV}^2$.

- The inelasticity y as measured from the hadronic activity in the detector using $y_h = \sum(E_i - p_{z,i})/(2E_e)$ must lie in the range $0.2 < y_h < 0.8$.

- Two jets with transverse momenta $p_T^{\mathrm{jet}1(2)} > 7(6)\,\mathrm{GeV}$ for the highest (second highest) p_T jet have to be found within the pseudorapitity range $-2.5 < \eta^{\mathrm{jet}} < 2.5$. Jets were identified by the inclusive k_t jet algorithm [19] in the p_T recombination scheme, with a distance parameter $R = 1.0$. The jet algorithm was applied in the laboratory frame, using hadronic final state objects combining track and calorimeter information.

- A muon, identified in the central muon system, with transverse momentum $p_T^\mu > 2.5\,\mathrm{GeV}$ has to be found in a pseudorapidity range $-0.55 < \eta^\mu < 1.1$. The muon has to be associated to one of the two highest energy jets.

To ensure a good muon reconstruction and suppress events with cosmic muons the following quality cuts were applied to the muon track:

- The muon must be identified in the Central Muon Detector CMD, i.e. it must have at least three hits in the ten layers of limited streamer tubes of the CMD. In events with several muon candidates, the one with the highest p_T^μ was selected.

- The χ^2 probability for the match between the CJC and the CMD tracks must be larger than $5\,\%$.

- The signed impact parameter of the muon[2] must lie in the range $-0.05 < \delta < 0.1\,\mathrm{cm}$ (this cut reduces background from cosmic muons and inflight decays of pions and kaons). The impact parameter is calculated with respect to the primary vertex of the event, which is determined from all tracks except the muon track.

---

[2]The sign of the impact parameter is determined in relation to the jet axis and defined such that it is positive for muons originating from a secondary vertex displaced along the jet direction.

- To reduce background from cosmic muons, the timing information of the CJC track must be consistent within $3\,\sigma$ (corresponding to $2.8\,\mathrm{ns}$) with the average event time[3].

- At least one hit in the CST must be linked to the CJC muon track.

- Events are rejected as cosmics where a second track in the opposite hemisphere fitting the muon candidate in ϕ and p_T is found.

5 Cross Section Definition and Measurement

We have measured the cross section of the process $ep \to e b \bar{b} X \to e j j \mu X'$, i.e. beauty production with the formation of two jets and the subsequent decay of a beauty hadron to a muon. The muon may be produced by a direct semileptonic decay of a beauty hadron, from a cascade decay, where the charm hadron decays semileptonically, or from a J/ψ or ψ' decay. The muon must be associated to either of the two highest p_T jets.

The visible range is defined by

$$
\begin{aligned}
Q^2 &< 1\,\mathrm{GeV}^2 \\
0.2 < y &< 0.8 \\
p_\mathrm{T}^\mu &> 2.5\,\mathrm{GeV} \\
-0.55 < \eta^\mu &< 1.1 \\
p_\mathrm{T}^{\mathrm{jet1(2)}} &> 7(6)\,\mathrm{GeV} \\
-2.5 < \eta^{\mathrm{jet1(2)}} &< 2.5.
\end{aligned}
$$

Events that pass the reconstruction cuts were binned differentially in one of the following quantities:

- The transverse momentum of the muon p_T^μ,

- the transverse momentum $p_\mathrm{T}^{\mathrm{jet1}}$ of the highest p_T jet,

- the pseudorapidity η^μ of the muon,

- x_γ^{obs}, the momentum fraction of the photon entering the hard interaction,

- and $\delta\phi_{\mathrm{jets}}$, the difference in azimuthal angle between the two jets.

To extract the beauty fraction, two quantities were used:

- $p_\mathrm{T}^{\mathrm{rel}}$ is the transverse momentum of the muon with respect to the axis of the most energetic jet, reconstructed without the muon four vector.

---

[3]For each event, a global T_0 is calculated from the CJC tracks; this T_0 is averaged over many events to give the average event time.

- δ is the impact parameter of the muon with respect to the primary vertex of the event.

For each bin, the two-dimensional distribution of these quantities were fitted with three template distributions derived from Monte Carlo simulations; these templates were generated separately for events containing only light (u, d, and s) quarks, charm quarks, and beauty quarks, respectively. The fit takes into account the statistical uncertainties from the data sample and the Monte Carlo templates [20, 21].

The result of the fit is the relative amount of beauty induced events f_b in each analysis bin, from which the observed number of beauty events N_b in the bin is calculated as $N_b = f_b \cdot N_{bin}$, where N_{bin} is the total number of data events observed in the respective bin; the data were then corrected for effects of detector resolution by a matrix unfolding procedure, with a migration matrix determined from Monte Carlo simulations.

5.1   Control Distributions

Fig. 1 shows control distributions of several important kinematic quantities for the selected sample: the muon transverse momentum p_T^μ and its pseudorapidity η^μ, the transverse momenta $p_T^{jet1(2)}$ of the highest and the second highest p_T jets, and the observable x_γ^{obs}. The data are compared to the PYTHIA Monte Carlo samples that were used to correct the data. The PYTHIA sample was reweighted as a function of the inelasticity y to improve the description of the data, and the relative fractions of light (uds), c and b quarks were adjusted to the values observed in the fit to the data. Overall, the description is very satisfactory.

Fig. 2 shows the distributions of the quantities used to extract the beauty fraction from the data: the impact parameter δ of the muon track and the transverse muon momentum p_T^{rel} relative to the axis of the associated jet. Both quantities are described quite well by the Monte Carlo simulation. In particular, the impact parameter distribution, which is very sensitive to the detector resolution, is very well described, in the region $\delta < 0$ that is dominated by resolution effects as well as in the region $\delta > 0$, which shows the tails due to long-lived particles from charm and beauty decays. This description has been achieved by careful tuning of the simulation software with regard to signal heights, noise levels and dead strips in the CST [22], the inclusion of effects from alignment imperfections, and the description of the dead material in front of the CST and the CJC. Further smearing of measured track parameters in the simulation is not necessary.

As can be seen from Fig. 2, events with beauty quarks, which already contribute at the level of $\approx 30\,\%$ to the sample, are enriched by cuts on the impact parameter or the relative p_T.

5.2   Systematic Uncertainties

A number of sources of systematic errors were considered. The following uncertainties contribute to the overall normalization uncertainty:

- The trigger efficiency,

- the identification of the muon in the instrumented iron,

- the efficiency to reconstruct the muon track in the tracking system and to link a CST hit,

- the luminosity.

Additional uncertainties affect the data differently in various bins:

- The impact parameter resolution,

- the reconstruction of the jet axis, which has an impact on the measurement of $p_{\mathrm{T}}^{\mathrm{rel}}$,

- the energy scale for hadrons of the calorimeter,

- the model uncertainties, estimated by using the Monte Carlo generator CASCADE [23] instead of PYTHIA 6.2 [7],

- the uncertainty from the fragmentation process, estimated by using the Lund [24] instead of the Peterson [12] fragmentation function,

- the uncertainty from the fragmentation fractions of c and b quarks into hadrons, their branching ratios and lifetimes,

- and the uncertainty on the modelling of π and K inflight decays.

The resulting systematic uncertainty is $12\,\%$.

6   Results

The total cross section for the process $ep \rightarrow eb\bar{b}X \rightarrow ejj\mu X'$ in the visible range given by $Q^2 < 1\,\mathrm{GeV}^2, 0.2 < y < 0.8, p_{\mathrm{T}}^{\mu} > 2.5\,\mathrm{GeV}, -0.55 < \eta^{\mu} < 1.1, p_{\mathrm{T}}^{\mathrm{jet1(2)}} > 7(6)\,\mathrm{GeV}$, and $-2.5 < \eta^{\mathrm{jet1(2)}} < 2.5$ has been measured to be

$$\sigma_{\mathrm{vis}}\left(ep \rightarrow eb\bar{b}X \rightarrow ejj\mu X'\right) = 31.4 \pm 1.3(stat.) \pm 3.8(syst.)\,\mathrm{pb}.$$

This result is somewhat lower than the published result [1] from HERA-I, which is

$$\sigma_{\mathrm{vis}}\left(ep \rightarrow eb\bar{b}X \rightarrow ejj\mu X'\right) = 38.4 \pm 3.4(stat.) \pm 5.4(syst.)\,\mathrm{pb},$$

but compatible within errors.

In comparison, the FMNR calculation yields

$$\sigma_{\mathrm{vis}}^{\mathrm{FMNR}}\left(ep \rightarrow eb\bar{b}X \rightarrow ejj\mu X'\right) = 25.3_{-4.7}^{+6.4}\,\mathrm{pb},$$

in agreement with the data, and the PYTHIA prediction is

$$\sigma_{\mathrm{vis}}^{\mathrm{PYTHIA}}\left(ep \rightarrow eb\bar{b}X \rightarrow ejj\mu X'\right) = 21.7\,\mathrm{pb}.$$

The differential cross sections also tend to be lower, but compatible, with the HERA-I results. The largest discrepancies are observed for the differential measurements in the lowest bins of p_T^μ and p_T^{jet1}, respectively. For these bins, the ratio between the HERA-II and the HERA-I measurements is about $2.5\,\sigma$ below unity if systematic uncertainties that do not cancel between both measurements are taken into account. It has been checked that this discrepancy is not caused by differences in the analysis method between the HERA-I and HERA-II analyses, such as different fitting procedures and different binnings in the two-dimensional fits used to extract the beauty fraction in each bin, or the fact the the new analysis uses an unfolding procedure to extract the differential cross section in p_T^{jet1}; we therefore attribute the difference to a statistical fluctuation.

Fig. 3a) shows the differential cross section as a function of the muon's pseudorapidity, η^μ. The measured values show little dependence on η^μ; in particular, there is no drop of the cross section in the forward direction, in contrast to PYTHIA and FMNR expectations.

In Fig. 3b), the dependence on the muon's transverse momentum, p_T^μ, is compared to the predictions. PYTHIA gives a steeper fall off than the data, while the NLO calculation describes the shape rather well.

The cross section also falls with the transverse momentum of the leading jet, p_T^{jet1}, albeit less steeply, as can be seen from Fig. 3c). The PYTHIA and FMNR calculations predict a rather similar behaviour and are both in agreement with the data.

Fig. 3d) shows the cross section as function of x_γ^{obs}, which approximates the photon's momentum entering the hard interaction. This observable is sensitive to the relative amounts of beauty produced in direct ($x_\gamma^{obs} \gtrsim 0.75$) and resolved ($x_\gamma^{obs} \lesssim 0.75$) photon processes. Here, the NLO calculation gives a good description of the data, while PYTHIA underestimates the relative amount of events at high x_γ^{obs}.

Finally, Fig. 3e) shows the difference in azimuthal angle, $\delta\phi_{jets}$, between the two jets. In leading order QCD the two outgoing quarks must be exactly opposite in azimuthal angle, corresponding to $\delta\phi_{jets} = 180°$. Thus, values of $\delta\phi_{jets}$ substantially lower than $180°$ are indicative of the presence of further final state gluons, and therefore this quantity is very sensitive to the description of gluon emission. PYTHIA, which employs parton showers to simulate the effect of multiple gluon emission, describes the shape of this observable reasonably well, as does the fixed order calculation of FMNR, which allows at most one hard gluon in the final state.

Overall, the data are reasonably well described in shape by the predictions from PYTHIA, but lie approximatly a factor 1.4 above the PYTHIA prediction.

The NLO predictions, derived with the FMNR program, also lie systematically below the data, but also describe the differential distributions well in shape. In particular, the deficiency in the lowest bins of p_T^μ and p_T^{jet1} is not substantially larger than in the other bins, in contrast to the findings of the HERA-I analysis.

This observation is in agreement with the result from an analysis [2] of HERA-I data by ZEUS, where good agreement with the FMNR predictions over the whole range in p_T^{jet1} and p_T^μ is found. In the ZEUS analysis, the same process is measured, albeit in a slightly different phase space (no cut on η^μ is made in the ZEUS analysis).

7 Conclusions

We have performed a measurement of the photoproduction of beauty quarks, using events where at least one beauty hadron decays with a muon in the final state, and two jets are visible in the detector. Beauty events are separated from background by means of the transverse momentum $p_T^{\rm rel}$ of the muon with respect to a jet, and by its impact parameter δ, utilizing the large lifetime of beauty hadrons. The measurement extends over the phase space region defined by $Q^2 < 1\,{\rm GeV}^2, 0.2 < y < 0.8, p_T^\mu > 2.5\,{\rm GeV}, -0.55 < \eta^\mu < 1.1, p_T^{\rm jet1(2)} > 7(6)\,{\rm GeV}$, and $-2.5 < \eta^{\rm jet1(2)} < 2.5$.

The visible cross section has been measured to be

$$\sigma_{\rm vis}\left(ep \to e b\bar{b}X \to ejj\mu X'\right) = 31.4 \pm 1.3(stat.) \pm 3.8(syst.)\,{\rm pb}.$$

A NLO QCD calculation is in agreement with this measurement within the theoretical uncertainties.

Differential cross sections have been measured as function of the observables η^μ, p_T^μ, $p_T^{\rm jet1}$, $x_\gamma^{\rm obs}$, and $\delta\phi_{\rm jets}$. The shape of these distributions is reasonably well described by the NLO QCD calculation as well as the PYTHIA LO Monte Carlo program.

At low values of p_T^μ and $p_T^{\rm jet1}$, the new measurement lies lower than the previous HERA-I measurement published by H1, and is thus better described by the NLO predictions than the previous measurement.

Acknowledgements

8 References

References

[1] A. Aktas *et al.* [H1 Collaboration], Eur. Phys. J. C **41** (2005) 453 [hep-ex/0502010].

[2] S. Chekanov *et al.* [ZEUS Collaboration], Phys. Rev. D **70** (2004) 012008 [Erratum-ibid. D **74** (2006) 059906] [hep-ex/0312057].

[3] I. Abt *et al.* [H1 Collaboration], Nucl. Instrum. Meth. A **386** (1997) 310 and 348.

[4] R. D. Appuhn *et al.* [H1 SpaCal Group], Nucl. Instrum. Meth. A **386** (1997) 397.

[5] D. Pitzl *et al.*, Nucl. Instrum. Meth. A **454** (2000) 334 [hep-ex/0002044];
     B. List, Nucl. Instrum. Meth. A **501** (2001) 49.

[6] A. Baird *et al.*, IEEE Trans. Nucl. Sci. **48** (2001) 1276 [hep-ex/0104010];
     A. Baird *et al.* [H1 Collaboration], Nucl. Instrum. Meth. A **461** (2001) 461;
     A. Schöning [H1 Collaboration], Nucl. Instrum. Meth. A **518** (2004) 542;
     N. Berger *et al.*, Nucl. Sc. Symp. Conf. Rec., 2004 IEEE, **3** (2004) 1976.

[7] T. Sjöstrand *et al.*, Comput. Phys. Commun. **135** (2001) 238 [hep-ph/0010017].

[8] R. Brun *et al.*, CERN-DD/EE–84–1 (1987).

[9] J. Pumplin *et al.*, JHEP **0207** (2002) 012 [hep-ph/0201195].

[10] G. A. Schuler and T. Sjöstrand, Phys. Lett. B **376** (1996) 193 [hep-ph/9601282].

[11] H. Jung, hep-ph/0411287 (2004).

[12] C. Peterson *et al.*, Phys. Rev. D **27** (1983) 105.

[13] S. Frixione, P. Nason and G. Ridolfi, Nucl. Phys. B **454** (1995) 3 [hep-ph/9506226].

[14] P. Nason, S. Dawson and R. K. Ellis, Nucl. Phys. B **303** (1988) 607;
     idem, Nucl. Phys. B **327** (1989) 49 [Erratum-ibid. B **335** (1990) 260];
     R. K. Ellis and P. Nason, Nucl. Phys. B **312** (1989) 551.

[15] W. M. Yao *et al.* [Particle Data Group], J. Phys. G **33** (2006) 1.

[16] H. L. Lai *et al.* [CTEQ Collaboration], Eur. Phys. J. C **12** (2000) 375 [hep-ph/9903282].

[17] M. Glück, E. Reya and A. Vogt, Phys. Rev. D **46** (1992) 1973.

[18] S. Alekhin *et al.*, hep-ph/0601013 (2006).

[19] S. D. Ellis and D. E. Soper, Phys. Rev. D **48** (1993) 3160 [hep-ph/9305266];
     M. Cacciari and G. P. Salam, Phys. Lett. B **641** (2006) 57 [hep-ph/0512210].

[20] R. J. Barlow and C. Beeston, Comput. Phys. Commun. **77** (1993) 219. Implemented in
     class TFractionFitter in the Root program.

[21] R. Brun *et al., "ROOT, an object oriented data analysis framework, user's guide 5.14,"*
     available at ftp://root.cern.ch/root/doc/Users_Guide_5_14.pdf.

[22] M. Krämer, *"Tuning the vertex detector simulation of H1,"* Proceedings of the Interna-
     tional School of Subnuclear Physics: 45th course: Search for the 'totally unexpected' in
     the LHC era. Erice, Sicily, 29.8.-7.9.2007.

[23] H. Jung and G. P. Salam, Eur. Phys. J. C **19** (2001) 351 [hep-ph/0012143];
     H. Jung, Comput. Phys. Commun. **143** (2002) 100 [hep-ph/0109102].

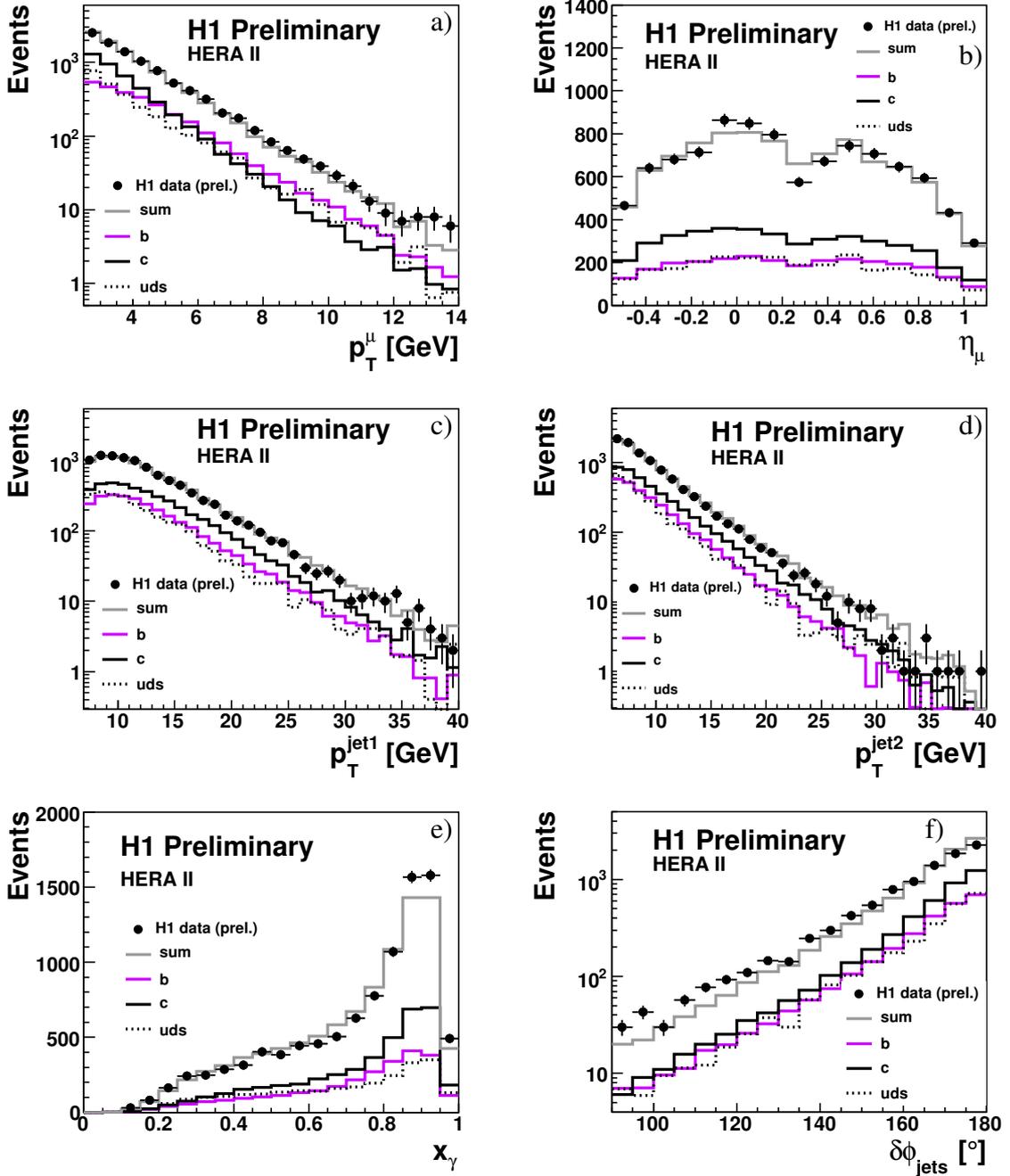[24] B. Andersson, G. Gustafson and B. Söderberg, Z. Phys. C **20** (1983) 317.

Figure 1: Distributions of a) the muon transverse momentum p_T^μ, b) the pseudorapidity of the muon η^μ, c) and d) the transverse momenta $p_T^{jet1(2)}$ of the highest and the second-highest p_T jets, respectively, e) the observable x_γ^{obs}, and f) the azimuthal angle between the jets, $\delta\phi_{jets}$. Included in the figure are the estimated contributions of events arising from beauty quarks (dark grey line), charm quarks (black line) and light quarks (dotted line). The shapes of the distributions from the different sources are taken from the PYTHIA Monte Carlo simulation and their relative fractions are determined from a fit to the two-dimensional data distribution of p_T^{rel} and the impact parameter δ (see text).
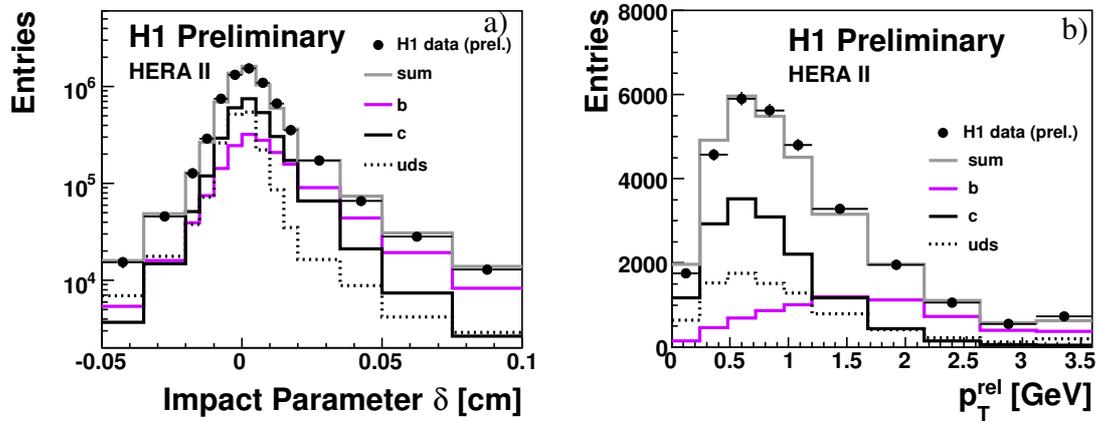
Figure 2: Distributions of a) the impact parameter δ of the muon track and b) the transverse muon momentum p_T^{rel} relative to the axis of the associated jet. Included in the figure are the estimated contributions of events arising from beauty quarks (dark grey line), charm quarks (black line) and light quarks (dotted line). The shapes of the distributions from the different sources are taken from the PYTHIA Monte Carlo simulation and their relative fractions are determined from a fit to the two-dimensional data distribution of p_T^{rel} t and the impact parameter δ (see text).
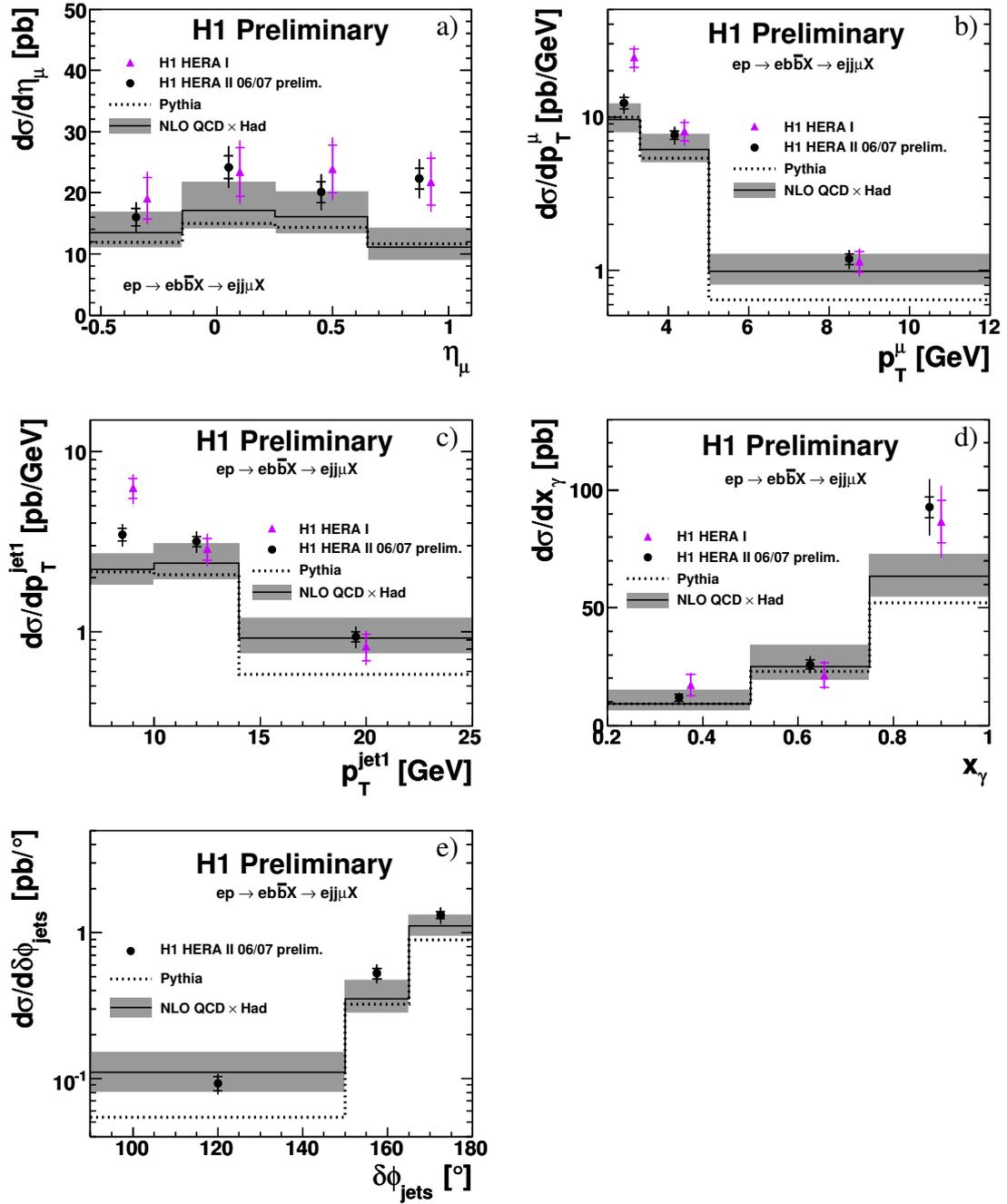
Figure 3: Differential cross sections for the photoproduction process $ep \rightarrow eb\bar{b}X \rightarrow ejj\mu X$ in the kinematic range $Q^2 < 1\,\mathrm{GeV}^2$, $0.2 < y < 0.8$, $p_T^\mu > 2.5\,\mathrm{GeV}$, $0.55 < \eta^\mu < 1.1$, $p_T^{\mathrm{jet1(2)}} > 7(6)\,\mathrm{GeV}$ and $|\eta^{\mathrm{jet1(2)}}| < 2.5$. The cross sections are shown as functions of a) the muon pseudorapidity η^μ, b) the muon transverse momentum p_T^μ, c) the jet transverse momentum p_T^{jet1} of the highest transverse momentum jet, d) the photon's momentum fraction x_γ^{obs} entering the hard interaction, and e) the azimuthal angle difference $\delta\phi_{\mathrm{jets}}$ between the jets. The inner error bars show the statistical error, the outer error bars represent the statistical and systematic uncertainties added in quadrature. The NLO QCD predictions are corrected to the hadron level (solid line) using the PYTHIA generator. The shaded band around the hadron level prediction indicates the systematic uncertainties as estimated from scale variations (see text). Predictions from the Monte Carlo generator PYTHIA (dotted line) are also shown.

12